

Powerful ordered collective heat engines

Fernando S. Filho,¹ Gustavo A. L. Forão,¹ D. M. Busiello,² B. Cleuren,³ and Carlos E. Fiore¹

¹Universidade de São Paulo, Instituto de Física, Rua do Matão, 1371, 05508-090 São Paulo, SP, Brazil

²Max Planck Institute for the Physics of Complex Systems, 01187 Dresden, Germany

³UHasselt, Faculty of Sciences, Theory Lab, Agoralaan, 3590 Diepenbeek, Belgium

(Dated: January 18, 2023)

We introduce a class of engines whereby units operating synchronously can be harnessed for leveraging its performance and also guiding the regime of operation. Our approach encompasses a minimal setup composed of N interacting unities placed in contact with two thermal baths and subjected to a constant driving worksource. The interplay between synchronized unities and optimal parameter choices provide maximal power and efficiency, the former and latter being able to reach Curzon-Ahlborn η_{CA} (including greater than η_{CA}) and Carnot η_c bounds, respectively. The main system features are captured by treating ordered effects through a phenomenological model and a linear analysis near the equilibrium regime. The present framework paves the way for the building of promising nonequilibrium thermal machines based on ordered structures.

Introduction. - The issue about building efficient engines is not only prominent but also pressing in thermodynamics since the pioneering work by Sadi Carnot [1] and has been strongly strengthened with the growing of nonequilibrium and quantum thermodynamics of small-scale engines [2, 3]. Unlike the standard Thermodynamics, fluctuations become fundamental in the such latter case and have its role subject of large attention, above all under (recent) experimental verifications [4–6]. As irreversibility is unavoidable, the efficiency generally decreases, illustrating the search for new strategies in the realm of nonequilibrium thermodynamics as crucial and strongly desirable. Bearing this in mind, a sort of distinct approaches has been proposed. Amidst them, we highlight the maximization of power [7–21] and efficiency [22, 23], thermodynamic control of the system-thermal bath interaction time [24, 25], its coupling [26] or even dynamics based on control via shortcuts to adiabaticity [27–29], to isothermality [30] and others [23, 31, 32].

The above examples/frameworks deal with engines composed of a single or few unities. However, several cases in nature encompass complex systems composed of many interacting unities, in which their cooperative effects are crucial. Among the most prominent specimen, we cite living [33–35], quantum [36–40] and biophysics systems [41], synchronization in network structures [42–46] and others, highlighting not only their importance but also how timely is the demand for growing and optimizing feasible, implementable, and robust strategies for engineered collective effects. Notwithstanding, the development, and performance of setups built from interacting unities is comparatively much less known and still remains at a primary stage [38, 47–50].

In this letter, we introduce a different class of collective effects, in which a synchronized operation under ordered arrangements plays a central role and can be harnessed for improving their performances. Inspired from ferromagnetic equilibrium models [51–54], we propose a minimal setup in which the power and efficiency can be enhanced via optimal choices of driving and couplings. Such main traits and optimization routes can be unveiled from a generic phenomenological description and linear analysis capturing all relevant marks.

Thermodynamics. - Since our goal aims at investigating the

essential features of the cooperative behavior from ordered arrays, we propose a generic system composed of N all-to-all interacting engines. Each microstate i is specified by the collection $N_{i\beta}$ of unities in each state β (for any β ranging from 1 to q) having dynamics governed by the master equation $\dot{p}_j = \sum_{\nu=1}^2 \sum_{i \neq j} (\omega_{ji}^{(\nu)} p_i - \omega_{ij}^{(\nu)} p_j)$, where $\omega_{ji}^{(\nu)}$ comprises the transition rate from i to j in which $N_{i\beta} \rightarrow N_{i\beta} - 1$ to $N_{i\beta'} \rightarrow N_{i\beta'} + 1$ ($\forall \beta' \in 1 \dots q$) due to the coupling with ν -th reservoir ($\nu = 1(2)$ for the cold(hot) bath with temperature $T_\nu = \beta_\nu^{-1}$). We assume transition rates as given by Arrhenius form $\omega_{ji}^{(\nu)} = \Gamma e^{-\frac{\beta_\nu}{2} (E_j - E_i + \sum_\gamma F_\gamma^{(\nu)} d_{ji}^{(\nu)})}$, with total energy E_i given by the generic all-to-all expression

$$E_i = \sum_{\beta=1}^q \epsilon_\beta N_{i\beta} + \frac{1}{2N} \sum_{(\beta, \beta' < \beta)}^q [\epsilon_{\beta\beta'} N_{i\beta} (N_{i\beta} - 1) + 2\epsilon_{\beta\beta'} N_{i\beta} N_{i\beta'}], \quad (1)$$

where ϵ_β , $\epsilon_{\beta\beta}$ and $\epsilon_{\beta\beta'}$ denote individual and interaction energies for the same and different state unities, respectively. Worksources originate from γ distinct driving forces $F_\gamma^{(\nu)}$'s with anti-symmetric weights $d_{ij}^{(\nu)}$ ($d_{ji}^{(\nu)} = -d_{ij}^{(\nu)}$). From above preliminaries the first law of thermodynamics is formulated from the time evolution of mean energy $\langle E \rangle = \sum_j E_j p_j$ given by $d\langle E \rangle/dt = \langle \dot{P} \rangle + \langle \dot{Q}_1 \rangle + \langle \dot{Q}_2 \rangle$, where the mean power $\langle \dot{P} \rangle$ and heat extracted exchanged with the ν -th thermal bath $\langle \dot{Q}_\nu \rangle$ are given by

$$\langle \dot{P} \rangle = - \sum_{(\nu, \gamma)} F_\gamma^{(\nu)} \sum_{(i, j)} d_{ji}^{(\nu)} J_{ji}^{(\nu)}, \quad (2)$$

$$\langle \dot{Q}_\nu \rangle = \sum_{(i, j)} \left(E_j - E_i + \sum_\gamma F_\gamma^{(\nu)} d_{ji}^{(\nu)} \right) J_{ji}^{(\nu)}, \quad (3)$$

respectively, expressed in terms of the probability current $J_{ij}^{(\nu)} = \omega_{ji}^{(\nu)} p_i - \omega_{ij}^{(\nu)} p_j$. The nonequilibrium steady state regime (NESS) is characterized by the set of steady probabilities $\{p_j^{\text{st}}\}$ in which $\langle \dot{P} \rangle + \langle \dot{Q}_1 \rangle + \langle \dot{Q}_2 \rangle = 0$, having the second law of thermodynamics expressed by the positiveness of entropy production

$$\langle \dot{\sigma} \rangle = \sum_{\nu=1}^2 \sum_{(i, j)} J_{ji}^{(\nu)} \ln \frac{\omega_{ji}^{(\nu)}}{\omega_{ij}^{(\nu)}} = -\beta_1 \langle \dot{Q}_1 \rangle - \beta_2 \langle \dot{Q}_2 \rangle, \quad (4)$$

where the right side was obtained by inserting the ratio $\omega_{ji}^{(v)}/\omega_{ij}^{(v)}$ into Eq. (4). Alternatively, $\langle \dot{\sigma} \rangle$ can be rewritten as $\langle \dot{\sigma} \rangle = \beta_1 \langle P \rangle + (\beta_1 - \beta_2) \langle \dot{Q}_2 \rangle$, allowing to characterize the engine performance through two (but equivalent) efficiency definitions: $\eta = -\langle P \rangle / \langle \dot{Q}_2 \rangle$ and/or from the above ratio between entropy production components $\hat{\eta} = -\eta_c^{-1} \langle P \rangle / \langle \dot{Q}_2 \rangle$, solely differing from each other for the Carnot bound $\eta_c = 1 - \beta_2/\beta_1$. A heat engine, which partially converts the heat extracted from the hot thermal bath ($\langle \dot{Q}_2 \rangle > 0$) into power output ($\langle P \rangle < 0$) is consistent to $\langle \dot{Q}_2 \rangle = -\langle P \rangle - \langle \dot{Q}_1 \rangle$ and hence $0 \leq \eta \leq \eta_c$ (or $0 \leq \hat{\eta} \leq 1$). Conversely, a pump regime is characterized by an amount of $\langle P \rangle > 0$ be partially consumed for extracting heat from the cold and to the hot bath (both $\langle \dot{Q}_v \rangle < 0$) and hence the condition $\langle P \rangle = -\langle \dot{Q}_2 \rangle - \langle \dot{Q}_1 \rangle$ is satisfied, implying that $\eta_c < \eta < \infty$ (or $1 < \hat{\eta} < \infty$). Finally, $\eta < 0$ for the dud regime.

The analysis will be carried out for finite N and $N \rightarrow \infty$. Since the achievement of steady probabilities become unfeasible as N increases (the number of configurations roughly increases with q^N), quantities have been calculated via generation of microscopic configurations according to the Gillespie algorithm [55] and checked (for the minimal setup of $N = 2$ engines) with the exact calculation of probability distribution via the solution of the master equation (see e.g. Fig. 4 in Supplemental Material). As described in Supplemental Material, for $N \rightarrow \infty$ the system is fully characterized by steady probabilities $p_\beta^{\text{st}} \rightarrow N_{i\beta}^{\text{st}}/N$ ($\beta = 1, \dots, q$) in which thermodynamic quantities acquire a similar form to Eqs. (2)-(4) and the master equation acquires a nonlinear form since probabilities appear in transition rates.

Minimal ordered collective heat engines and phenomenological description.- Eq. (1) offers a large avenue of $2q + q(q-1)/2$ distinct parameters to be considered. For simplicity, the influence of number of states per unity will be exploited by curbing our analysis for $q = 2$ and 3 which can be mapped into general spin models $S = 1/2$ ($\{\downarrow, \uparrow\}$) and $S = 1$ ($\{\downarrow, 0, \uparrow\}$), respectively. We take a two-fold choice for $\epsilon_{\beta\beta'}$'s, which has been inspired by two of the main cornerstones systems conceived for describing ferromagnetic-paramagnetic phase transitions in magnetic materials: Ising and Potts models [51, 56, 57]. In the former and latter cases, one has $\epsilon_{\uparrow\uparrow} = \epsilon_{\downarrow\downarrow} = \epsilon$, $\epsilon_{\uparrow\downarrow} = -\alpha\epsilon$ and $\epsilon_{\beta\beta'} = \epsilon\delta_{\beta,\beta'}$ (for all β and β'), respectively, where we take equal ϵ_β 's and all remaining parameters are set as zero. For the sake of clarity, the former and latter choices will be referred from now on as engine A and B, respectively, whose expressions for transition rates are shown in Supplemental material. Inspired in kinesin models [58, 59] and other engine setups [47, 48], the worksource is implemented by introducing a bias for the occurrence of certain transitions, as specified in Fig. 1 (Fig. 2 in Supplemental Material) for $q = 3$ ($q = 2$), respectively. This is accomplished by allowing the variable $d_{ij}^{(v)}$ to assume two values, $d_{ij}^{(v)} = (-1)^v$ according to whether the transition from j to i is clockwise or counterclockwise and depending on the thermal bath it is coupled. For simplicity, we consider only one kind of driving $\gamma = 1$ and $F_\gamma^{(v)} = F$ for both v .

Figs. 1 depicts the main features of engines A and B for $q = 3$ and $N \rightarrow \infty$ (from now on, all quantities will be cal-

culated for $\Gamma = 1$). Unities will evolve to one of the ordered phases depending on the initial configuration, for sufficiently (large) $\epsilon < 0$, being two-fold in all cases (except for model B, $q = 3$, which is three-fold). A heat engine is present for the model A and finite F whenever $p_\downarrow^{\text{st}}(p_\uparrow^{\text{st}})$ dominates over the remaining p_α^{st} 's for $F > 0$ ($F < 0$). Associate efficiencies η 's and power-outputs per unity \mathcal{P} 's increase upon ϵ is raised reaching maximum performances η_{ME} and \mathcal{P}_{MP} at optimal couplings ϵ_{ME} and ϵ_{MP} , respectively. As exemplified in Fig. 1(a), maximum efficiency approach to the ideal limit η_c at ϵ_{ME} as α is large (for all α) for engine A and $q = 3$ ($q = 2$), revealing the reliability of our strategy for obtaining efficient engines under nonequilibrium conditions. Ordered arrays also permit unities to be projected as a pump for large F 's, as illustrated in panel Fig. 1(c). Contrasting with the engine A and with work-to-work transducers [48, 49], no heat regime is present for model B and $q = 3$, irrespective of parameters (see e.g. Fig. 1(e)), in which only a pump operation is possible, provided unities operate independently. Analogous findings are depicted in Fig. 2 (Supplemental Material) for $q = 2$.

To tackle our main discoveries, we develop a phenomenological description in which steady probabilities are treated via (approximate) expressions $p_\downarrow^{\text{st}} = 1 - \gamma e^{\delta x}$ and $p_\uparrow^{\text{st}} = \gamma e^{\delta x}$ where $x = \epsilon/F$ and parameters γ and δ solely depend on β_1, β_2 and F/ϵ . As described in Supplemental Material, the measure of system synchronization is given by the quantity $-M = p_\downarrow^{\text{st}} - p_\uparrow^{\text{st}} = 1 - 2\gamma e^{\delta x} > 0$ for $q = 2$, which it is close to 1. It is worth mentioning that $|M|$ reduces to $|M| \approx 1 - e^{\beta\epsilon}$ in the equilibrium regime ($\beta_1 = \beta_2$ and $F = 0$), consistent to the magnetization per spin $M = \tanh(\beta\epsilon M/2)$ of the Ising model for sufficient low temperatures ($\beta \gg \beta_c = \epsilon/k_B$) and $H = 0$ [51, 57]. From expressions in Supplemental Material, one arrives at the phenomenological generic expressions for power \mathcal{P}_{ph} and heat $\langle \dot{Q}_2 \rangle_{ph}$ per unity for $q = 2$:

$$\mathcal{P}_{ph} = \frac{F}{2} e^{-\frac{1}{2}\beta_2[(\alpha+1)\epsilon M + F]} \left[e^{\frac{1}{2}[(\beta_1+\beta_2)F - (\beta_1-\beta_2)(\alpha+1)\epsilon M]} - 1 \right] \times \left[(1+M)e^{\frac{1}{2}[-(\beta_1-\beta_2)F + (\beta_1+\beta_2)(\alpha+1)\epsilon M]} - M + 1 \right], \quad (5)$$

and

$$\langle \dot{Q}_2 \rangle_{ph} = -(F + (\alpha+1)M\epsilon) \left[\sinh\left(\frac{\beta_2}{2}(F + (\alpha+1)M\epsilon)\right) + M \cosh\left(\frac{\beta_2}{2}(F + (\alpha+1)M\epsilon)\right) \right], \quad (6)$$

respectively, where the efficiency is given by the ratio between the above quantities. Our phenomenological description is promptly adapted for the model A and $q = 3$, but now p_0^{st} reads $p_0^{\text{st}} = \gamma e^{\delta x}$ and the p_\uparrow^{st} is approximately neglected. Thermodynamic quantities per unity in such case read:

$$\mathcal{P}_{ph} = F \left[(1+M) \left(e^{\frac{1}{2}\beta_1(F-\alpha M\epsilon)} - e^{-\frac{1}{2}\beta_2(F+\alpha M\epsilon)} - e^{-\frac{1}{2}\beta_1(F-M\epsilon)} + e^{\frac{1}{2}\beta_2(F+M\epsilon)} \right) - M \left(e^{\frac{1}{2}\beta_1(F-M\epsilon)} - e^{-\frac{1}{2}\beta_2(F+M\epsilon)} - e^{-\frac{1}{2}\beta_1(F+(\alpha+1)M\epsilon)} + e^{\frac{1}{2}\beta_2(F-(\alpha+1)M\epsilon)} \right) \right], \quad (7)$$

and

$$\langle \dot{Q}_2 \rangle_{ph} = -(1+M) \left[(F + M\epsilon) e^{\frac{1}{2}\beta_2(F+M\epsilon)} - (F + \alpha M\epsilon) e^{-\frac{1}{2}\beta_2(F+\alpha M\epsilon)} + M \left[(F - (\alpha+1)M\epsilon) e^{\frac{1}{2}\beta_2(F-(\alpha+1)M\epsilon)} - (F + M\epsilon) e^{-\frac{1}{2}\beta_2(F+M\epsilon)} \right] \right], \quad (8)$$

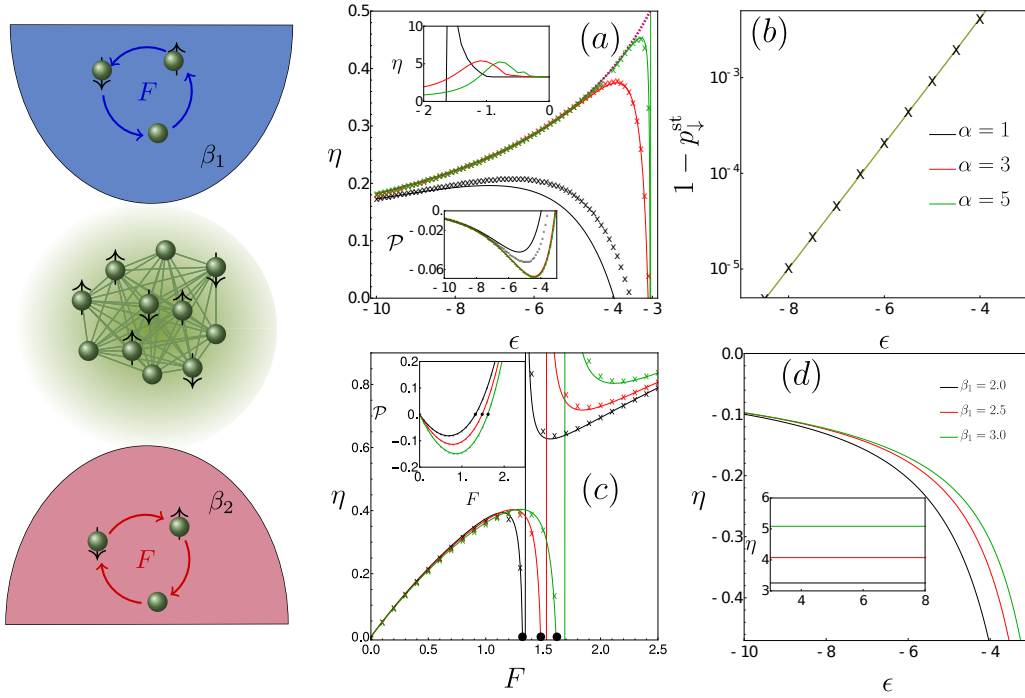


FIG. 1. Left: Schematics of $q = 3$ engines for generic interactions among unities. For model A and distinct α 's, panel (a) depicts the efficiency η versus coupling ϵ in the regime of strong (a) and weak (top inset) collective effects. Purple lines denote the efficiency evaluated from Eq. (9). In the bottom inset, the corresponding power outputs \mathcal{P} 's per unity. For the same parameters from (a), panel (b) illustrates the reliability of the phenomenological description (symbols) through a monolog plot of $1 - p_t^{st}$ versus ϵ respectively. Parameters in (a) and (b): $\beta_1 = 2, \beta_2 = 1$ and $F = 1$. The influence of driving forces is exhibited in panel (c) by depicting η and \mathcal{P} per unity versus F for distinct β_1 's, where vertical lines (specified by a \bullet) mark the crossover between heat engine and pump regimes. Parameters in (c): $\alpha = 3, \epsilon = -4, \beta_2 = 1$. As previously, symbols \times correspond to the phenomenological description from Eqs. (7) and (8). Panel (d) exemplifies, for the same temperatures as in (c) and $F = 1$, the absence of heat machine regime for model B in the regime of collective effects. Inset: Efficiencies at the pump regime operation when unities operate independently.

respectively, where $-M = p_{\downarrow}^{st} - p_{\uparrow}^{st} = 1 - \gamma e^{\delta x} > 0$. Efficiency is straightforwardly evaluated from the ratio between above quantities, acquiring a simpler form for large α and $q = 3$ given by

$$\eta_{ph} = \frac{F}{F + M\epsilon} \left[1 - \frac{\exp\{-\frac{\beta_1}{2}(F - M\epsilon)\} + 2M \cosh\{\frac{\beta_1}{2}(F - M\epsilon)\}}{\exp\{\frac{\beta_2}{2}(F + M\epsilon)\} + 2M \cosh\{\frac{\beta_2}{2}(F + M\epsilon)\}} \right]. \quad (9)$$

The reliability of Eqs. (7)-(9) is depicted in Fig. 1 (symbols) providing a very good description of both heat engine [(a),(c) for small F] and pump [(c) for larger F] regimes. However, small discrepancies are present for small α . This is due to the fact that although p_{\uparrow}^{st} is very small ($p_{\uparrow}^{st} \sim O(10^{-9})$), it is not negligible. Similar findings for $q = 2$ are depicted in Supplemental Material. The extension of the above discoveries for other ϵ 's and F 's are shown in Fig. 2 for $q = 3$. The heat engine and pump regimes are separated by an intermediate region in which unities work dudly. Both of them can be maximized with respect to F for fixed ϵ and vice-versa. Maximum lines are promptly obtained from expressions for \mathcal{P} or η or via the phenomenological description. Contrasting with the efficiency, power-output heat maps are always marked by a central region providing \mathcal{P}_{MP}^* (simultaneous maximization with respect to ϵ and F), which is precisely the crossing between continuous and dotted lines. Conversely, no simultaneous maximization of efficiency is presented and the engine

operates more efficiently as $-\epsilon$ and F increase. Above general trademarks also appear in the linear regime (near the equilibrium regime, e.g. $\beta_1 - \beta_2 \ll 1$ and $F \ll 1$), in which the entropy production acquires a bilinear form and it is expressed in terms of Onsager coefficients. As described in Supplemental Material, in such a case maximum efficiency η_{ME} and efficiency at maximum power η_{MP} solely depend on the coupling parameter $\kappa = L_{12}/\sqrt{L_{11}L_{22}}$. Giving that $|\kappa|$ monotonically increases with ϵ , both η_{ME} and η_{MP} approach to their ideal values for strong collective effects ($\kappa \rightarrow -1$).

As suggested in Fig. 1, an alternative route for optimization is carried out for finite ϵ, F and larger values of α . Fig. 3 extends such a point by depicting maximum efficiencies versus α . While η_{ME} approaches to ideal η_c , efficiencies at global maximum power η_{MP}^* approach to Curzon Ahlborn bound $\eta_{CA} = 1 - \sqrt{\beta_2/\beta_1}$ upon α is raised ($\eta_{CA} = 0.2929...$ for $\beta_2 = 1$ and $\beta_1 = 2$) and corresponding efficiencies at maximum power η_{MP} becomes greater than η_{CA} .

Many versus few interacting unities.- Aforementioned discoveries were depicted for $N \rightarrow \infty$ interacting unities. Despite the fraction of unities operating under ordered ways plays an important role for leveraging the machine performance, above hallmarks are presented for setups composed of finite systems, as exemplified in Fig. 4 for engine A for $q = 3$

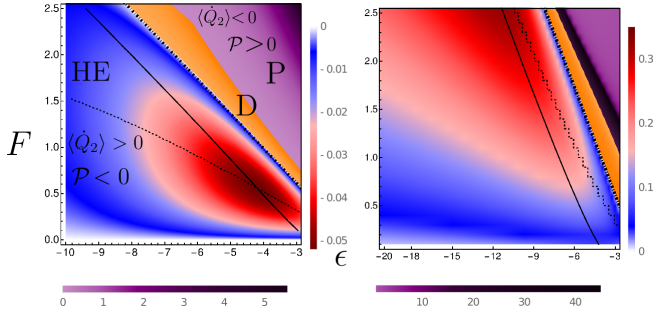


FIG. 2. For the model A for $q = 3$, the power and efficiency heat maps. Symbols HE , P and D account for the heat engine, pump and dud regimes, respectively. Continuous and dotted lines denote maximizations of \mathcal{P} for F and ϵ held fixed, respectively. Dashed lines state the crossover from heat engine to dud regimes. Parameters: $\beta_1 = 2, \beta_2 = \alpha = 1$.

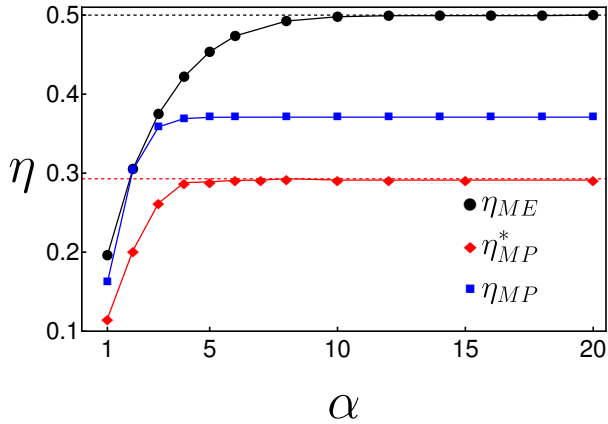


FIG. 3. Maximum efficiency η_{ME} (black circles), efficiency at maximum power η_{MP} (blue squares) and efficiency at global maximum power η_{MP}^* (red diamonds) versus α . The black and red dashed lines correspond Carnot η_c and Curzon-Ahlborn η_{CA} efficiencies, respectively.

and distinct N 's, even for the minimal $N = 2$ setup (see e.g. Supplemental material for more details). Apart from the reduced performances for smaller system sizes (including a reduced heat engine range), it is worth underlining that, they "quickly" approach to the asymptotic limit $N \rightarrow \infty$ as N increases, including the well description via the phenomenological approach. It should also be noted the existence of some range of values of ϵ in which the engine performance is superior for finite N than for $N \rightarrow \infty$. Since $\langle \dot{Q}_2 \rangle / N$ monotonically decreases with N , such behavior is due to the a larger absolute value of $\mathcal{P} = \langle P \rangle / N$ in such intervals. Similar findings are found for $q = 2$ (see e.g. Fig. 2 in Supplemental Material). Therefore, the stochastic dynamics and thermodynamics of finite N approach to that for $N \rightarrow \infty$ for sufficiently long times, in a similar behavior with work-to-work transducers considered in [48].

Crossover from heat to pump engine regimes and phase transitions.- As stated before, collective effects allow unities

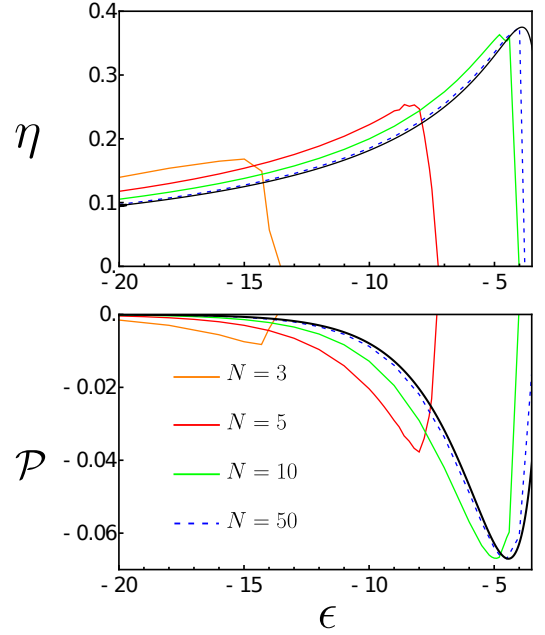


FIG. 4. The depiction of efficiency η and power per unity $\mathcal{P} = \langle P \rangle / N$ at the heat regime for distinct system sizes N for $\alpha = 3$. The black continuous line represents the $N \rightarrow \infty$ case. Parameters: $\beta_1 = 2, \beta_2 = 1$ and $F = 1$.

to be projected as a pump upon F is increased. A pump regime also emerges from the other way around to collective effects, in which unities operate almost (or fully) independently. The crossover between synchronized and independent operation mode always takes place from threshold coupling ϵ_c , manifesting under different ways, such as discontinuous ($q = 2$ and engine B for $q = 3$), continuous phase transitions (engine A for $q = 3$ and $\alpha = 1$) and by crossovers absent of phase transitions (remaining cases). Although exact in all cases, the independent mode operation only yields for finite ϵ for engines A and B (for $\alpha = 1$) when $q = 3$. In such cases, expressions for \mathcal{P} and $\langle \dot{Q}_v \rangle$'s per unity are given by

$$\mathcal{P} = 2F \left[\sinh\left(\frac{F\beta_1}{2}\right) + \sinh\left(\frac{F\beta_2}{2}\right) \right] \quad \text{and} \quad (10)$$

$$\langle \dot{Q}_v \rangle = -2F \sinh\left(\frac{F\beta_v}{2}\right), \quad (11)$$

respectively, both being independent on ϵ . Similar expressions are obtained for $q = 2$ and $\epsilon \rightarrow \infty$, solely differing from them by factor 2 and all of them state that only a pump regime operation is possible, with efficiency in the previous cases given by $1/\eta = 1 + \sinh(\beta_1 F/2) / \sinh(\beta_2 F/2)$. Figs. 1-2 depict the above main features for $q = 3$ (see Supplemental Material for $q = 2$). Despite a pump regime coming from collective and independent operations, the interaction in the former case can always be conveniently chosen for promoting a better performance than independent ones, reinforcing again the importance of collective effects.

Conclusions.- We introduced a minimal class of reliable thermal engines in which their operation in a synchronized way can exhibit distinct regimes, maximal powers and ef-

iciencies, notably ideal values under nonequilibrium conditions. Despite the non-trivial interplay between interaction, driving, and collective effects, all main features can be extracted from a generic phenomenological model and a linear analysis. The overall approach is general and opens the door to exciting directions for future research. Firstly, the extension to distinct lattice topologies might be important not only for building more realistic and (maybe) more efficient setups, but also for stating the reliability of all-to-all interactions. Furthermore, it will be valuable to draw a comparison with other engine projections, such as sequential ones, in which the sys-

tem is subjected to distinct conditions at each stroke, instead of simultaneous ones. Finally, the achievement of feasible bounds for the power, efficiency and dissipation, expressed in terms of currents and system interactions, can provide important information about collective effects.

Acknowledgments- Authors are grateful to Pedro Harunari for useful suggestions and comments. This work has received the financial support from CAPES and FAPESP under grants 2021/03372-2 and 2021/13287-2, respectively.

Supplemental Material: Powerful ordered collective heat engines

Fernando S. Filho, Gustavo A. L. Forão, D. M. Busiello, Bart Cleuren and C. E. Fiore

This supplemental material is structured as follows: In Sec. A we describe the transition rates for finite N and $N \rightarrow \infty$ interacting unities. In Sec. B, we derive a heuristic argument for steady probabilities in the regime of strong collective effects as a function of $\beta_1, \beta_2, \epsilon$ and the F . The main results for $q = 2$ engines and the analysis of a minimal setup composed of $N = 2$ ($q = 3$) interacting engines are shown in Secs. C and D, respectively. The system features near the equilibrium regime are investigated in Sec. E. As a side analysis, the linear stability of the disordered solution for $q = 3$ is investigated in Sec. F.

Appendix A: Transition rates

As stated in the main text, collective effects from ordered structures have been investigated for two models for $q = 2$ and $q = 3$. They can be grouped in a common expression for $q = 2$, in which engine B is precisely set by $\alpha = 0$. The system dynamics is governed by the master equation $\dot{p}_j = \sum_{v=1}^2 \sum_{i \neq j} (\omega_{ji}^{(v)} p_i - \omega_{ij}^{(v)} p_j)$, where transition rates i to j are given by

$$\omega_{ji}^{(1)} = \Gamma e^{-\frac{\beta_1}{2} \{\mp \epsilon(1+\alpha)(1 - \frac{2N_{i\uparrow(\downarrow)} \mp 1}{N}) \mp F\}} \quad \text{and} \quad \omega_{ji}^{(2)} = \Gamma e^{-\frac{\beta_2}{2} \{\mp \epsilon(1+\alpha)(1 - \frac{2N_{i\downarrow(\uparrow)} \mp 1}{N}) \pm F\}}, \quad (\text{A1})$$

where signs $\mp \epsilon(1 + \alpha)$ attempt for the transition from state i to j in which $N_{i\uparrow} \rightarrow N_{i\uparrow} \pm 1$ and $N_{i\downarrow} \rightarrow N_{i\downarrow} \mp 1$, respectively, with associate driving contribution $\mp F$ and $\pm F$ due to the contact with the cold ($v = 1$) and hot ($v = 2$) thermal baths, respectively. For a given N , the dynamics is generated from Gillespie algorithm [55] in which each above transition is chosen with probability $\omega_{ji}^{(v)} / \tilde{w}$, where $\tilde{w} = \Gamma \left(N_{i\uparrow} e^{-\frac{\beta_1}{2} \{\epsilon(1+\alpha)(1 - \frac{2N_{i\uparrow}+1}{N}) + F\}} + N_{i\uparrow} e^{-\frac{\beta_2}{2} \{\epsilon(1+\alpha)(1 - \frac{2N_{i\uparrow}+1}{N}) - F\}} + N_{i\downarrow} e^{-\frac{\beta_1}{2} \{\epsilon(1+\alpha)(1 - \frac{2N_{i\downarrow}+1}{N}) - F\}} + N_{i\downarrow} e^{-\frac{\beta_2}{2} \{\epsilon(1+\alpha)(1 - \frac{2N_{i\downarrow}+1}{N}) + F\}} \right)$.

The thermodynamic limit $N \rightarrow \infty$ is obtained by replacing $N_{i\uparrow(\downarrow)} / N \rightarrow p_{\uparrow(\downarrow)}$, in which the time evolution of probability p_β [$\beta \in (\downarrow, \uparrow)$] is ruled by the master equation $\dot{p}_\beta = \sum_{v=1}^2 J_{\beta\beta'}^{(v)}$, where $J_{\beta\beta'}^{(v)} = \omega_{\beta\beta'}^{(v)} p_{\beta'} - \omega_{\beta'\beta}^{(v)} p_\beta$ with transition rates listed below:

$$\omega_{\uparrow\downarrow}^{(1)} = \Gamma e^{-\frac{\beta_1}{2} \{-\epsilon(1+\alpha)(1-2p_\uparrow) - F\}} \quad \text{and} \quad \omega_{\uparrow\downarrow}^{(2)} = \Gamma e^{-\frac{\beta_2}{2} \{-\epsilon(1+\alpha)(1-2p_\uparrow) + F\}}, \quad (\text{A2})$$

for $(\beta', \beta) \equiv (\downarrow, \uparrow)$ and

$$\omega_{\downarrow\uparrow}^{(1)} = \Gamma e^{-\frac{\beta_1}{2} \{\epsilon(1+\alpha)(1-2p_\uparrow) + F\}} \quad \text{and} \quad \omega_{\downarrow\uparrow}^{(2)} = \Gamma e^{-\frac{\beta_2}{2} \{\epsilon(1+\alpha)(1-2p_\uparrow) - F\}}, \quad (\text{A3})$$

for $(\beta, \beta') \equiv (\downarrow, \uparrow)$ respectively.

Transition rates are evaluated in a similar fashion for $q = 3$, in which energy differences can be grouped in three distinct sets. Starting with engine A, they are identical to $q = 2$ for transitions of type $\uparrow(\downarrow) \rightarrow \downarrow(\uparrow)$, whereas the energy difference reads $\epsilon(N_{ik} - \alpha N_{i\ell})/N$ for transitions like $0 \rightarrow \uparrow(\downarrow)$, where $k = \uparrow(\downarrow)$ and $\ell = \downarrow(\uparrow)$ (likewise for all other ways round of transitions). Likewise, for engine B, a given transition $N_{i\ell} \rightarrow N_{i\ell} - 1$ and $N_{ik} \rightarrow N_{ik} + 1$ (where $k, \ell \in (\uparrow, 0, \downarrow)$) has energy difference given by $\epsilon(N_{ik} - N_{i\ell} + 1)/N$ [48, 49]. Numerical simulations are performed as before, but now there are $2q(q-1) = 12$ distinct transitions. As for $q = 2$, the limit $N \rightarrow \infty$ is promptly obtained and described by the master equation $\dot{p}_\beta = \sum_{v=1}^2 \sum_{\beta' \neq \beta} J_{\beta\beta'}^{(v)}$ [$\beta \in (\downarrow, 0, \uparrow)$], but now there are six distinct transitions. Below, we list some of them:

$$\omega_{\uparrow\downarrow}^{(1)} = \Gamma e^{-\frac{\beta_1}{2} \{-\epsilon(1+\alpha)(p_\downarrow - p_\uparrow) + F\}}, \quad \omega_{\uparrow 0}^{(1)} = \Gamma e^{-\frac{\beta_1}{2} \{\epsilon(p_\uparrow - \alpha p_\downarrow) - F\}} \quad \text{and} \quad \omega_{0\downarrow}^{(1)} = \Gamma e^{-\frac{\beta_1}{2} \{\epsilon(\alpha p_\uparrow - p_\downarrow) - F\}}, \quad (\text{A4})$$

for engine A and

$$\omega_{\uparrow\downarrow}^{(1)} = \Gamma e^{-\frac{\beta_1}{2} \{\epsilon(p_\uparrow - p_\downarrow) + F\}}, \quad \omega_{\uparrow 0}^{(1)} = \Gamma e^{-\frac{\beta_1}{2} \{\epsilon(p_\uparrow - p_0) - F\}} \quad \text{and} \quad \omega_{0\downarrow}^{(1)} = \Gamma e^{-\frac{\beta_1}{2} \{\epsilon(p_0 - p_\downarrow) - F\}}, \quad (\text{A5})$$

for engine B, where in all cases the limit $N_{ij}/N \rightarrow p_\beta$ was taken. The remaining transitions are calculated analogously and corresponding $\omega_{ij}^{(2)}$'s are promptly obtained from $\omega_{ij}^{(1)}$'s just by replacing $F \rightarrow -F$. Finally, thermodynamic quantities expressions in the limit $N \rightarrow \infty$ are similar to those presented in the main text (for finite N), where the power \mathcal{P} and heat $\langle \dot{Q}_v \rangle$ per unity are given by

$$\mathcal{P} = - \sum_{(\nu, \gamma)} F_\gamma^{(\nu)} \sum_{(\beta, \beta')} d_{\beta\beta'}^{(\nu)} J_{\beta\beta'}^{(\nu)} \quad \text{and} \quad \langle \dot{Q}_v \rangle = \sum_{(\beta, \beta')} \left(E_\beta - E_{\beta'} + \sum_\gamma F_\gamma^{(\nu)} d_{\beta\beta'}^{(\nu)} \right) J_{\beta\beta'}^{(\nu)}, \quad (\text{A6})$$

where the energy difference $E_\beta - E_{\beta'}$ was evaluated previously for each transition.

Appendix B: Phenomenological description for the probability distribution in the regime of strong collective effects

Despite the nonlinear shape of the master equation for $N \rightarrow \infty$, it is possible to get some insight about the probability distribution in the regime of strong collective effects, as described as follows. Starting with $q = 2$, the ordered phase has degeneracy 2 and characterized by the predominance of a spin of type ($p_\downarrow^{st} \gg p_\uparrow^{st}$ or $p_\uparrow^{st} \gg p_\downarrow^{st}$). By focusing on the former solution, steady probabilities are approximately given by

$$p_\downarrow^{st} \approx \frac{\omega_{\downarrow\uparrow}^{(1)} + \omega_{\downarrow\uparrow}^{(2)}}{\omega_{\downarrow\uparrow}^{(1)} + \omega_{\downarrow\uparrow}^{(2)} + \omega_{\uparrow\downarrow}^{(1)} + \omega_{\uparrow\downarrow}^{(2)}}, \quad (\text{B1})$$

where $p_\uparrow^{st} = 1 - p_\downarrow^{st}$ and, at this level of approximation, the probabilities p_\uparrow^{st} and p_\downarrow^{st} appearing in transition rates have been neglected. Taking into account that $\beta_2 < \beta_1$, $F > 0$ and $-\epsilon \gg F$ (strong collective effects), it follows that $\omega_{\downarrow\uparrow}^{(2)} > \omega_{\downarrow\uparrow}^{(1)} \gg \omega_{\uparrow\downarrow}^{(1)} > \omega_{\uparrow\downarrow}^{(2)}$ and Eq. (B1) is approximately given by $p_\downarrow^{st} \approx 1 - (\omega_{\uparrow\downarrow}^{(1)} + \omega_{\uparrow\downarrow}^{(2)})/(\omega_{\downarrow\uparrow}^{(1)} + \omega_{\downarrow\uparrow}^{(2)})$. Since $\omega_{\downarrow\uparrow}^{(2)} > \omega_{\downarrow\uparrow}^{(1)}$ and $\omega_{\uparrow\downarrow}^{(1)} > \omega_{\uparrow\downarrow}^{(2)}$, the ratio $\omega_{\uparrow\downarrow}^{(1)}/\omega_{\uparrow\downarrow}^{(2)}$ is dominant and finally p_\downarrow^{st} acquires the simpler form $p_\downarrow^{st} \approx 1 - e^{\frac{1}{2}[(\beta_1 + \beta_2)(1 + \alpha)\epsilon]} e^{\frac{(\beta_1 - \beta_2)F}{2}}$, where $\epsilon < 0$. Note that it has the general form $p_\downarrow^{st} = 1 - \gamma e^{\delta x}$ described in the main text, where $\delta = (\beta_1 + \beta_2)(1 + \alpha)/2$ and $\gamma = \exp(\beta_1 - \beta_2)F/2$ for $x = \epsilon$ and $\delta = (\beta_1 - \beta_2)/2$ and $\gamma = \exp[(\beta_1 + \beta_1)(1 + \alpha)\epsilon/2]$ for $x = F$.

By inserting above expressions for p_\downarrow^{st} and p_\uparrow^{st} into expressions from Eq. (A6), one arrives at the following expressions for $\mathcal{P}_{ph} \equiv \mathcal{P}$ and $\langle \dot{Q}_2 \rangle_{ph} \equiv \langle \dot{Q}_2 \rangle$ described in the main text. All similar procedures can be extended for $q = 3$ just by replacing $\uparrow \rightarrow 0$ and neglecting the other transition rates. In this case, $p_\downarrow^{st} \approx 1 - \omega_{0\downarrow}^{(1)}/\omega_{0\downarrow}^{(2)} = 1 - e^{\frac{1}{2}[(\beta_1 + \beta_2)\epsilon + (\beta_1 - \beta_2)F]}$. Fig. 5 exemplifies the validity of approximate expression for p_\downarrow^{st} for distinct sets of temperatures β_1, β_2 and F for $q = 3$.

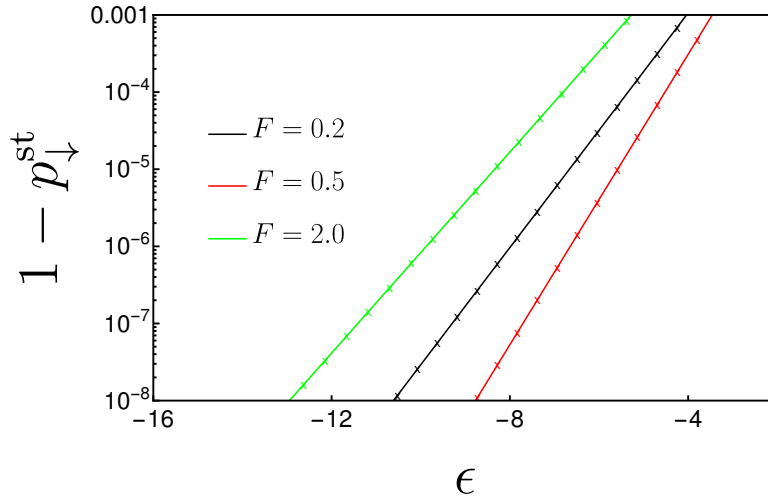


FIG. 5. Monolog plot of $1 - p_\downarrow^{st}$ versus ϵ for distinct sets of β_1, β_2 and F . Continuous lines and symbols denote exact results for $N \rightarrow \infty$ and those from expression $1 - p_\downarrow^{st} = e^{\frac{(\beta_1 + \beta_2)\epsilon + (\beta_1 - \beta_2)F}{2}}$, respectively.

Appendix C: Thermodynamics of $q=2$ engines

The main features of the thermodynamics of $q = 2$ engines are summarized in Figs. 6 and 7. The former shows, for finite N and $N \rightarrow \infty$, the power per unity, efficiency and reliability of the two-state the model discussed in the main text:

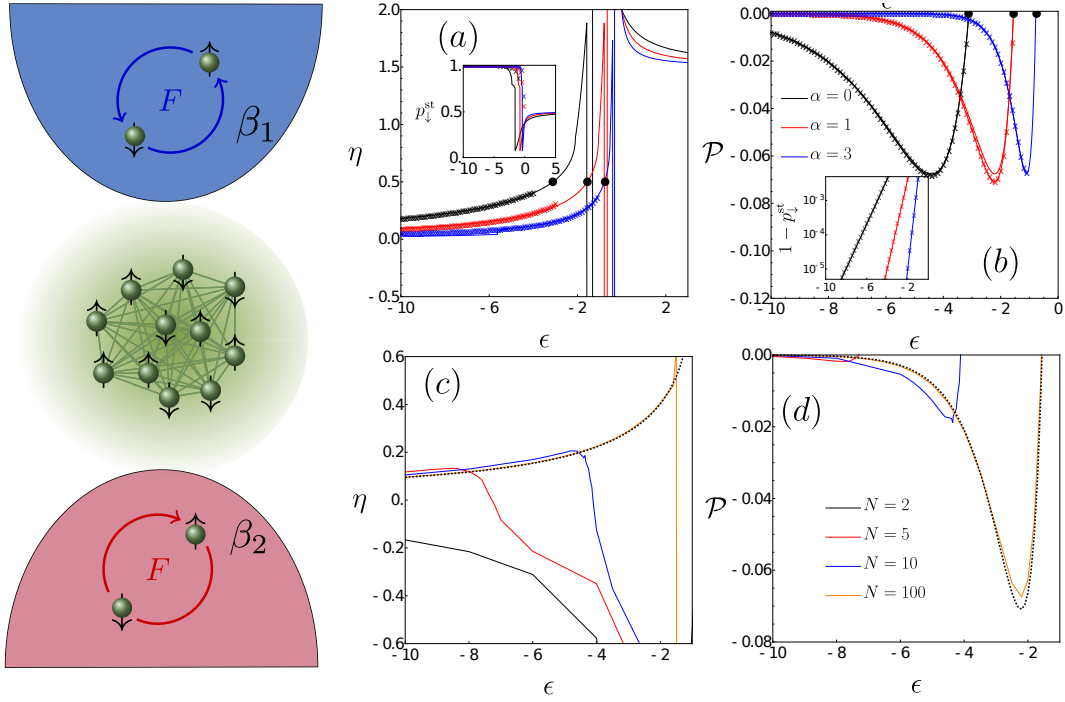


FIG. 6. Left: Schematics of the driving operation for $q = 2$ engines. For $\beta_1 = 2, \beta_2 = F = 1$ and distinct α 's, panels (a)-(b) depict the efficiency η and the power per unity \mathcal{P} versus interaction strength ϵ , respectively. Circles show the optimal ϵ_{ME} 's in which $\eta = \eta_c$. In both cases, symbols correspond to the phenomenological description. Insets: plot of p_d^{st} and monolog plot p_t versus ϵ , respectively. For the same parameters as in the top panels, the bottom panels show $\mathcal{P} = \langle \mathcal{P} \rangle / N$ and η for finite N 's and $\alpha = 1$.

Fig. 7 extends the power and efficiency heat maps for $\alpha = 1$. Note the similar behavior to $q = 3$, but in this case ideal heat engine operations are obtained for all values of α at ϵ_{ME} (F fixed) or F_{ME} (ϵ fixed). They satisfy the conditions $\mathcal{P} = \langle \dot{Q}_2 \rangle = 0$ and according to the two-state model, ideal efficiencies (dashed lines) fulfill the condition $M = -\tanh\left[\frac{\beta_2}{2}(F + (\alpha + 1)M\epsilon)\right]$ at ϵ_{ME}/F_{ME} when F/ϵ is held fixed.

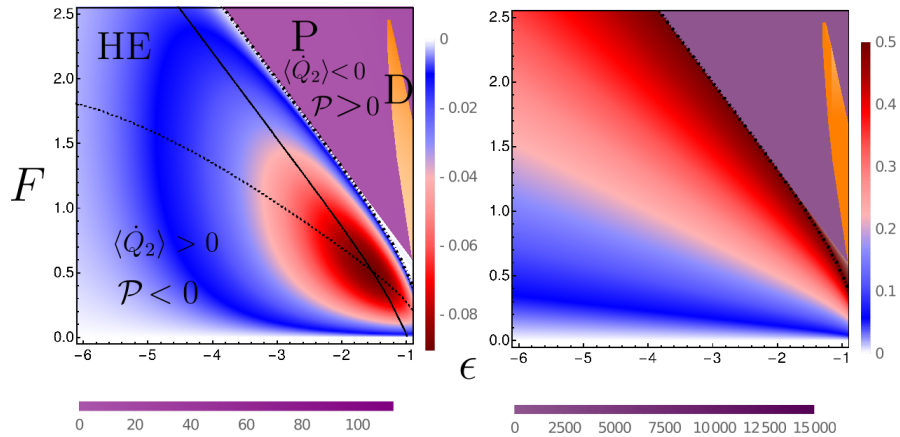


FIG. 7. For the same parameters from Fig. 6, the heat maps for the \mathcal{P} and η . Heat engine, pump, and dud regimes are described by symbols HE , P , and D , respectively. Continuous and dotted lines denote maximizations of power for F and ϵ held fixed, respectively. The dashed line corresponds to the crossover from heat engine to pump regimes, in which $\eta = \eta_c$.

Appendix D: Heat maps for $q=3$ and $N=2$ engines

This section portrays two important aspects discussed in the main text: the reliability of numerical simulations for finite N and the fact a minimal setup of $N = 2$ interacting unities already captures the essential ingredients introduced here. For such a minimal setup, collective effects are measured by a dominant fraction of quantity $-M = p_{\downarrow\downarrow}^{st} - p_{\uparrow\uparrow}^{st}$.

In both cases, results will be shown for $\beta_1 = 1$ and $\beta_2 = 0.4$, in which the engine performance is somewhat superior to $\beta_1 = 2$ and $\beta_2 = 1$. The former aspect is depicted in Fig. 8 by comparing thermodynamic quantities evaluated from numerical simulations (Gillespie algorithm) and those from exact steady probabilities via largest eigenvalue of the master equation.

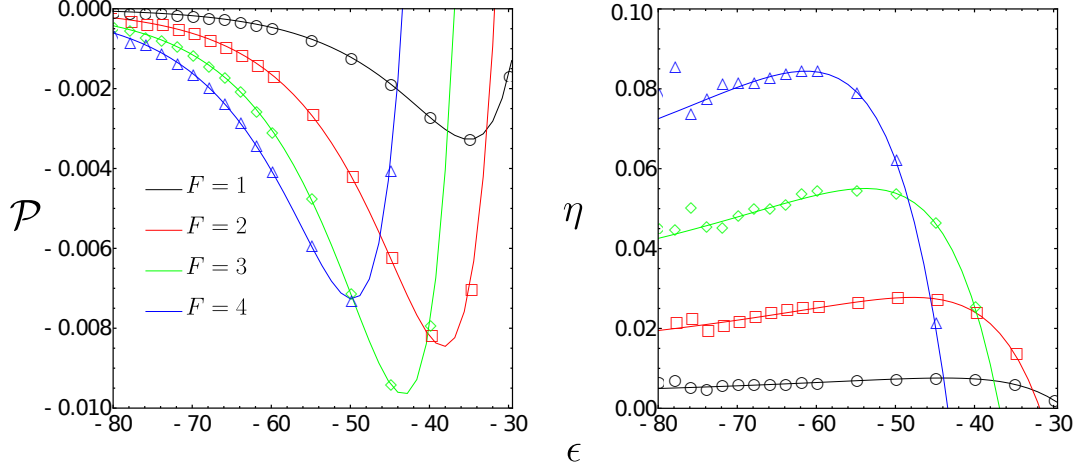


FIG. 8. Left and right panels show the power per unity $\mathcal{P} = \langle P \rangle / N$ and efficiency for $N = 2$. Continuous lines and symbols show the comparison between the exact solution, via exact probability distribution, and numerical simulations from Gillespie algorithm, respectively.

Fig. 9 extends the heat maps for the minimal setup of $N = 2$, showing that despite the substantial reduced performance, all characteristics from collective effects are already present in the minimum $N = 2$ setup.

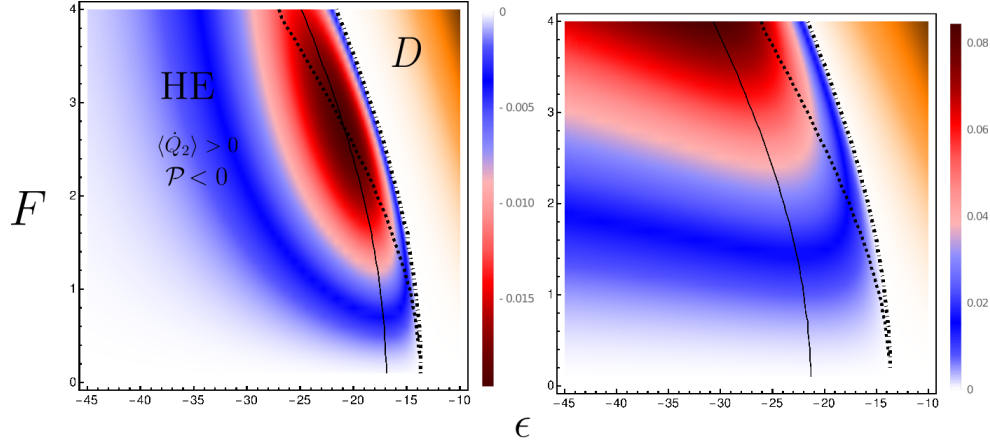


FIG. 9. For $q = 3$ and $N = 2$, top panels depict power per unity $\mathcal{P} = \langle P \rangle / N$ and efficiency heat maps, respectively. Heat engine and dud regimes are described by symbols *HE* and *D*, respectively. For a better visualization the pump regime has been omitted. Parameters: $\alpha = 1$, $\beta_1 = 1$ and $\beta_2 = 0.4$.

Appendix E: Linear regime

Additional insights regarding the influence of the collective effects on the efficiency and power are obtained from a linear analysis, valid near equilibrium ($\beta_1 - \beta_2$, $F \ll 1$). By resorting to the linear stochastic thermodynamics ideas [56, 60–63], one

introduces the following thermodynamic forces $f_1 = \beta_1 - \beta_2$ and $f_2 = \beta_1 F$, in such a way that the entropy production $\langle \dot{\sigma} \rangle$ is expressed in the bilinear form

$$\langle \dot{\sigma} \rangle = (\beta_1 - \beta_2) \langle \dot{Q}_2 \rangle + \beta_1 \mathcal{P} = J_1 f_1 + J_2 f_2, \quad (\text{E1})$$

where $J_1 = \langle \dot{Q}_2 \rangle$ and $J_2 = \mathcal{P}/F$ denote the thermodynamic fluxes. Near equilibrium, ie. in the linear regime, these fluxes can be expressed in terms of the Onsager coefficients, $J_1 = L_{11}f_1 + L_{12}f_2$ and $J_2 = L_{21}f_1 + L_{22}f_2$, which satisfy the conditions $L_{11}, L_{22} \geq 0$ and $L_{12} = L_{21}$. From the above, the efficiency $\hat{\eta}$ promptly reads

$$\hat{\eta} = -\frac{\beta_1 \mathcal{P}}{(\beta_1 - \beta_2) \langle \dot{Q}_2 \rangle} = -\frac{L_{21}f_2f_1 + L_{22}f_2^2}{L_{11}f_1^2 + L_{12}f_1f_2}, \quad (\text{E2})$$

from which $\eta = \hat{\eta}\eta_c$ follows immediately. As previously, the heat engine ($\mathcal{P} < 0$) or pump ($\mathcal{P} > 0$) regimes impose boundaries to optimization with respect to f_2 , whose absolute value must lie in the interval $0 \leq |f_2| \leq |f_m|$, where $f_m = -L_{21}f_1/L_{22}$ the so-called stopping force for which $\mathcal{P} = 0$. As previously, the optimization can be performed to ensure maximum power \mathcal{P}_{MP} (with efficiency η_{MP}) or maximum efficiency η_{ME} (with power \mathcal{P}_{ME}), by adjusting the output force f_2 to optimal values $f_{2,\text{MP}}$ and $f_{2,\text{ME}}$, respectively. These optimal output forces can be expressed in terms of the Onsager coefficients as

$$f_{2,\text{ME}} = \frac{L_{11}}{L_{12}} \left(-1 + \sqrt{1 - \frac{L_{12}^2}{L_{11}L_{22}}} \right) f_1, \quad (\text{E3})$$

and

$$f_{2,\text{MP}} = -\frac{1}{2} \frac{L_{12}}{L_{22}} f_1, \quad (\text{E4})$$

respectively, where the property $L_{21} = L_{12}$ has been considered. By inserting $f_{2,\text{ME}}$ or $f_{2,\text{MP}}$ into expressions for $\hat{\eta}$, we obtain $\hat{\eta}_{\text{ME}}$ and the efficiency at maximum power $\hat{\eta}_{\text{MP}}$ given by,

$$\hat{\eta}_{\text{ME}} = -1 + \frac{2L_{11}L_{22}}{L_{12}^2} \left(1 - \sqrt{1 - \frac{L_{12}^2}{L_{11}L_{22}}} \right), \quad (\text{E5})$$

and

$$\hat{\eta}_{\text{MP}} = \frac{L_{12}^2}{4L_{11}L_{22} - 2L_{12}^2}, \quad (\text{E6})$$

and similarly the expressions for \mathcal{P}_{MP} and \mathcal{P}_{ME} are obtained. In fact, these quantities are not independent of each other, instead they are related as

$$\hat{\eta}_{\text{MP}} = \frac{\hat{\eta}_{\text{ME}}}{1 + \hat{\eta}_{\text{ME}}^2} \quad \text{and} \quad \frac{\mathcal{P}_{\text{ME}}}{\mathcal{P}_{\text{MP}}} = 1 - \hat{\eta}_{\text{ME}}^2, \quad (\text{E7})$$

where the symmetry between crossed Onsager coefficients $L_{12} = L_{21}$ was taken into account. It is convenient to introduce the coupling parameter $\kappa = L_{12}/\sqrt{L_{11}L_{22}}$ [9, 64], in such a way that maximum efficiencies $\hat{\eta}_{\text{MP}}$ and $\hat{\eta}_{\text{ME}}$ are solely expressed in terms of κ given by

$$\hat{\eta}_{\text{ME}} = -1 + \frac{2}{\kappa^2} (1 - \sqrt{1 - \kappa^2}), \quad (\text{E8})$$

and

$$\hat{\eta}_{\text{MP}} = \frac{1}{2} \frac{\kappa^2}{2 - \kappa^2}, \quad (\text{E9})$$

respectively. Since $\langle \dot{\sigma} \rangle \geq 0$, it follows that κ must be constrained in the interval $-1 \leq \kappa \leq 1$, implying that both $\hat{\eta}_{\text{MP}}$ and $\hat{\eta}_{\text{ME}}$ are confined to $0 \leq \hat{\eta}_{\text{MP}} \leq 1/2$ and $0 \leq \hat{\eta}_{\text{ME}} \leq 1$, respectively. Notice that $\kappa = \pm 1$ corresponds to the determinant of the (2×2) Onsager Matrix being equal to zero. And this, in turn, implies proportionality between the two thermodynamic fluxes, $J_1 \propto J_2$, for all forces f_1 and f_2 . Fig. 10 shows that all signatures about collective effects are also captured by the linear regime, describing very well the system behavior near the equilibrium regime (panels (b) and (c)). Remarkably, the increase of efficiencies toward the ideal case as ϵ and driving force goes up described in the main text is understood from the interplay among L_{ij} 's in which the coupling $|\kappa|$ monotonously increases toward the ideal limit $\kappa \rightarrow -1$ (panel (a) and inset). Also, $\hat{\eta}_{\text{ME}}$ and $\hat{\eta}_{\text{MP}}$ follow Eqs. (E8)-(E9) (d).

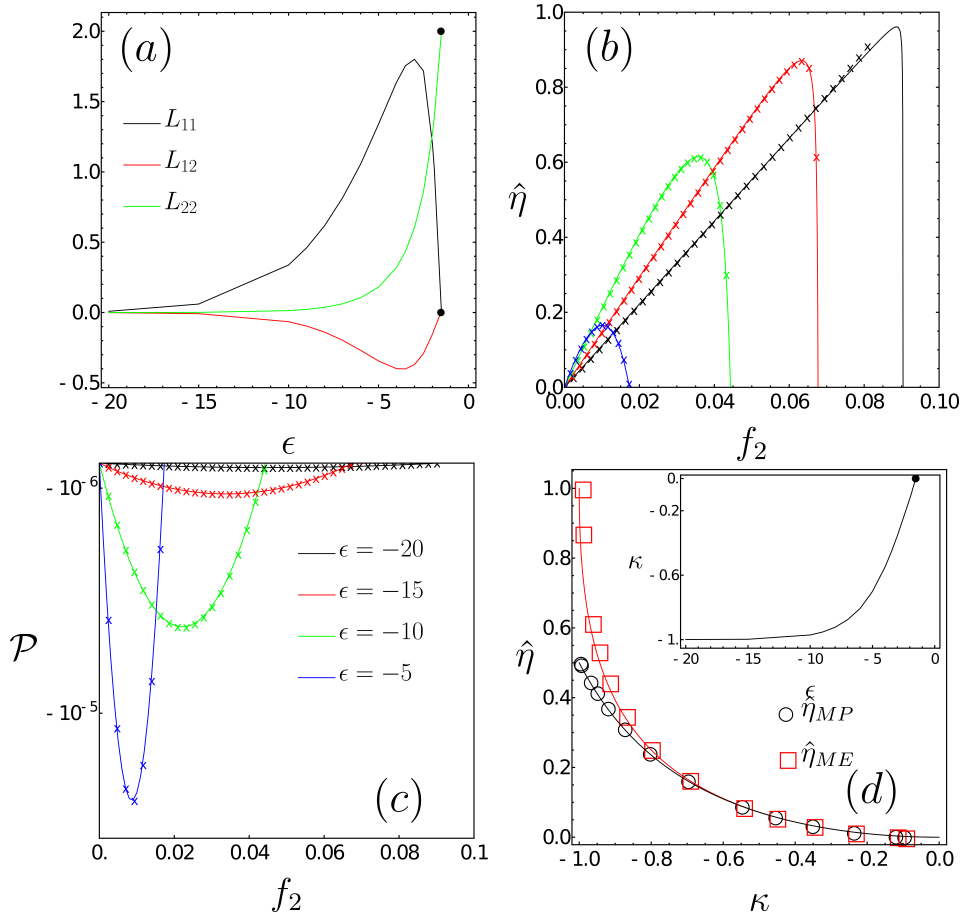


FIG. 10. For engine A, $q = 3$ and $\alpha = 1$, the depiction of system thermodynamics near the equilibrium regime. Panel (a) and inset show the Onsager coefficients L_{ij} 's and coupling κ versus interaction parameter ϵ . In (b) and (c) shows $\hat{\eta}$ and \mathcal{P} versus f_2 for $f_1 = 9 \cdot 10^{-3}$. Continuous lines and symbols correspond to exact results and those obtained from Eq. (E2), respectively. Each heat engine is delimited by vertical lines yielding at f_m . Panel (d) shows the behavior of maximum efficiency $\hat{\eta}_{ME}$ and efficiency at maximum power $\hat{\eta}_{MP}$ versus κ , where continuous lines follow Eqs. (E8) and (E9), respectively. The symbol \bullet denotes the crossover to the independent regime yielding at $\epsilon_c \approx -1.5$.

Appendix F: Linear stability of disordered phase solution for models A and B for $q=3$

For completeness, we provide additional information about the crossover between collective and independent regimes for engines A (for $\alpha = 1$) and B for $q = 3$ which manifests through continuous and discontinuous phase transitions, respectively. They can be analyzed in a similar way to their equilibrium counterparts, by means of order parameters M and $\phi = 3(p_{max} - 1)/2$ ($p_{max} = \max\{p_{\downarrow}^{st}, p_0^{st}, p_{\uparrow}^{st}\}$), respectively, the former one characterized by the classical exponent $\beta = 1/2$ [65, 66]. However, contrasting to the equilibrium Potts model, nonequilibrium ingredients shift the phase transition for engine B, from continuous to discontinuous, as exemplified in panel (b) of Fig. 11. Alternatively, both phase transitions can be investigated under a linear expansion of master equation given by $\dot{p}_m = \sum_n A_{mn} p_n$, where A is the Jacobian matrix with elements $A_{mn} = \partial(\omega_{mn}^{(1)} + \omega_{mn}^{(2)})/\partial p_n|_{p_n=p^*}$ evaluated at fixed points $\sum_n A_{mn} p_n^* = 0$ for $n = 0, \uparrow$ (where $p_{\downarrow}^* = 1 - p_{\uparrow}^* - p_0^*$). In particular, the solution p_n^* is linearly stable if real parts of eigenvalues of Jacobian matrix are negative [67]. In both cases, the independent regime is characterized by equal population $p_{\downarrow}^* = p_0^* = p_{\uparrow}^* = 1/3$ for $\epsilon \geq \epsilon_c$, in which associate eigenvalues can be written as $\lambda_{\pm} = \lambda_0 \pm \lambda_1$, with λ_0 , in both cases, given by

$$\lambda_0 = -(3 + \beta_1 \epsilon) \cosh\left(\frac{\beta_1 F}{2}\right) - (3 + \beta_2 \epsilon) \cosh\left(\frac{\beta_2 F}{2}\right), \quad (F1)$$

whereas λ_1 's read

$$\lambda_1 = \left[6 + \epsilon^2 (\beta_1^2 + \beta_2^2) + (\beta_1^2 \epsilon^2 - 3) \cosh(\beta_1 F) - 3 \cosh(\beta_2 F) + \beta_2 \epsilon^2 \left(4\beta_1 \cosh\left(\frac{\beta_1 F}{2}\right) \cosh\left(\frac{\beta_2 F}{2}\right) + \beta_2 \cosh(\beta_2 F) \right) + 12 \sinh\left(\frac{\beta_1 F}{2}\right) \sinh\left(\frac{\beta_2 F}{2}\right) \right]^{1/2}, \quad (\text{F2})$$

for engine A and

$$\lambda_1 = i \sqrt{3} \left[\sinh\left(\frac{\beta_1 F}{2}\right) - \sinh\left(\frac{\beta_2 F}{2}\right) \right], \quad (\text{F3})$$

for engine B, respectively. Since λ_1 is imaginary for engine B, the linear stability of disordered solution is granted provided $\lambda_0 < 0$. Conversely, for engine A, due to the fact that β_1 and β_2 are always positive, λ_- is always negative. Conversely, λ_+ is always positive (negative) for sufficiently $\epsilon < 0$ ($\epsilon \geq 0$), respectively, in which the order-disorder phase transition corresponds to a transcritical bifurcation when $\lambda_+ = 0$.

Fig. 11 depicts the phase diagrams $\Delta\beta = \beta_1 - \beta_2$ versus ϵ_c for different F obtained from the linear analysis. In particular, for $F = 0$, both λ_+ 's and λ_- 's read -6 and $-2[3 + \epsilon(\beta_1 + \beta_2)]$ (engine A) and $-[6 + \epsilon(\beta_1 + \beta_2)]$ (engine B), respectively, consistent to phase transitions yielding at $\epsilon_c = -3/(\beta_1 + \beta_2)$ and $\epsilon_c = -6/(\beta_1 + \beta_2)$. The crossover from collective to independent regime smoothly changes with the driving and it is more sensitive to the difference of temperatures. Note the excellent agreement between ϵ_c 's obtained from linear analysis and those from order parameter behaviors (bottom panels for $F = 1$).

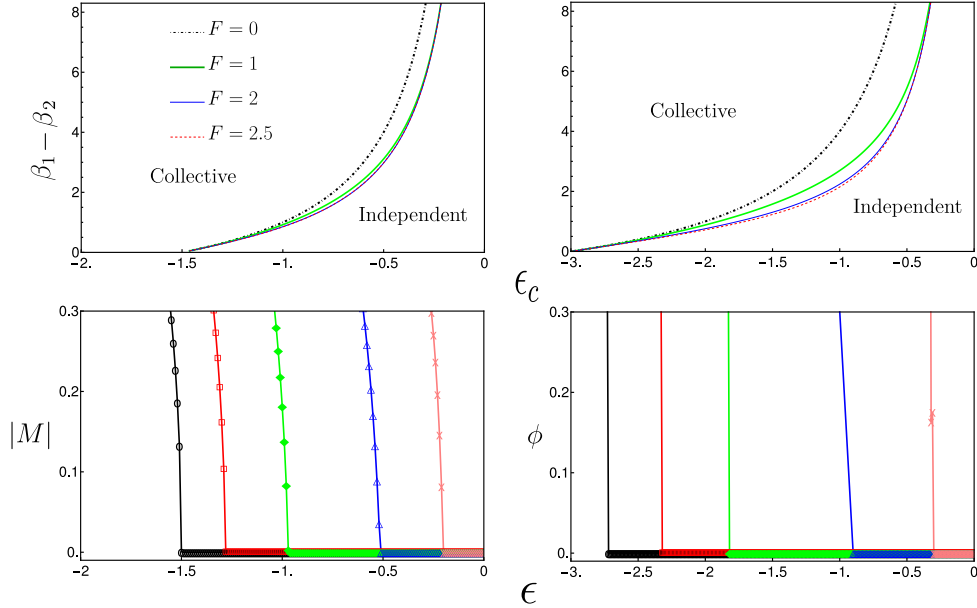


FIG. 11. For $q = 3$ and distinct F 's, left and right panels depict the phase diagrams $\Delta\beta = \beta_1 - \beta_2$ versus ϵ_c for engines A and B, respectively, obtained from the linear stability of the disordered phase. For the sake of comparison, the bottom panels show (for $F = 1$) the location of phase transitions from order-parameter behaviors. From left to right $\beta_1 - \beta_2 = 0, 1/3, 1, 3$ and 9 . In all cases, we set $\beta_2 = 1$.

-
- [1] S. Carnot, *Réflexions sur la puissance motrice du feu*, 26 (Vrin, 1978).
 - [2] F. Curzon and B. Ahlborn, *American Journal of Physics* **43**, 22 (1975).
 - [3] U. Seifert, *Reports on progress in physics* **75**, 126001 (2012).
 - [4] D. Collin, F. Ritort, C. Jarzynski, S. B. Smith, I. Tinoco, and C. Bustamante, *Nature* **437**, 231 (2005).
 - [5] T. P. Xiong, L. L. Yan, F. Zhou, K. Rehan, D. F. Liang, L. Chen, W. L. Yang, Z. H. Ma, M. Feng, and V. Vedral, *Phys. Rev. Lett.* **120**, 010601 (2018).
 - [6] L.-L. Yan, J.-W. Zhang, M.-R. Yun, J.-C. Li, G.-Y. Ding, J.-F. Wei, J.-T. Bu, B. Wang, L. Chen, S.-L. Su, F. Zhou, Y. Jia, E.-J. Liang, and M. Feng, *Phys. Rev. Lett.* **128**, 050603 (2022).
 - [7] G. Verley, M. Esposito, T. Willaert, and C. Van den Broeck, *Nature Communications* **5**, 4721 (2014).
 - [8] T. Schmiedl and U. Seifert, *Europhysics Letters* **81**, 20003 (2007).
 - [9] B. Cleuren, B. Rutten, and C. Van den Broeck, *The European*

- Physical Journal Special Topics **224**, 879 (2015).
- [10] C. Van den Broeck, Physical Review Letters **95**, 190602 (2005).
 - [11] M. Esposito, R. Kawai, K. Lindenberg, and C. Van den Broeck, Physical Review E **81**, 041106 (2010).
 - [12] U. Seifert, Physical Review Letters **106**, 020601 (2011).
 - [13] Y. Izumida and K. Okuda, Europhysics Letters **97**, 10004 (2012).
 - [14] N. Golubeva and A. Imparato, Physical Review Letters **109**, 190602 (2012).
 - [15] V. Holubec, Journal of Statistical Mechanics: Theory and Experiment **2014**, P05022 (2014).
 - [16] M. Bauer, K. Brandner, and U. Seifert, Physical Review E **93**, 042112 (2016).
 - [17] K. Proesmans, B. Cleuren, and C. Van den Broeck, [Physical review letters](#) **116**, 220601 (2016).
 - [18] Z. Tu, Journal of Physics A: Mathematical and Theoretical **41**, 312003 (2008).
 - [19] S. Ciliberto, Physical Review X **7**, 021051 (2017).
 - [20] M. V. S. Bonança, [Journal of Statistical Mechanics: Theory and Experiment](#) **2019**, 123203 (2019).
 - [21] B. Rutten, M. Esposito, and B. Cleuren, Physical Review B **80**, 235122 (2009).
 - [22] K. Proesmans, B. Cleuren, and C. Van den Broeck, [Physical review letters](#) **116**, 220601 (2016).
 - [23] I. N. Mamede, P. E. Harunari, B. A. N. Akasaki, K. Proesmans, and C. E. Fiore, [Phys. Rev. E](#) **105**, 024106 (2022).
 - [24] C. E. F. Noa, A. L. L. Stable, W. G. C. Oropesa, A. Rosas, and C. E. Fiore, [Phys. Rev. Research](#) **3**, 043152 (2021).
 - [25] P. E. Harunari, F. S. Filho, C. E. Fiore, and A. Rosas, [Phys. Rev. Research](#) **3**, 023194 (2021).
 - [26] P. Talkner and P. Hänggi, [Rev. Mod. Phys.](#) **92**, 041002 (2020).
 - [27] D. Guéry-Odelin, A. Ruschhaupt, A. Kiely, E. Torrontegui, S. Martínez-Garaot, and J. G. Muga, [Rev. Mod. Phys.](#) **91**, 045001 (2019).
 - [28] S. Deffner and M. V. Bonança, [EPL \(Europhysics Letters\)](#) **131**, 20001 (2020).
 - [29] N. Pancotti, M. Scandi, M. T. Mitchison, and M. Perarnau-Llobet, Physical Review X **10**, 031015 (2020).
 - [30] X.-H. Zhao, Z.-N. Gong, and Z. C. Tu, “Microscopic low-dissipation heat engine via shortcuts to adiabaticity and shortcuts to isothermality,” (2022).
 - [31] H. C. Fogedby and A. Imparato, [EPL \(Europhysics Letters\)](#) **119**, 50007 (2017).
 - [32] A. Imparato, Journal of Statistical Mechanics: Theory and Experiment **2021**, 013214 (2021).
 - [33] F. S. Gnesotto, F. Mura, J. Gladrow, and C. P. Broedersz, Reports on Progress in Physics **81**, 066601 (2018).
 - [34] C. W. Lynn, E. J. Cornblath, L. Papadopoulos, M. A. Bertolero, and D. S. Bassett, Proceedings of the National Academy of Sciences **118**, e2109889118 (2021).
 - [35] P. Smith and M. Schuster, Current Biology **29**, R442 (2019).
 - [36] G. Kurizki, P. Bertet, Y. Kubo, K. Mølmer, D. Petrosyan, P. Rabl, and J. Schmiedmayer, Proceedings of the National Academy of Sciences **112**, 3866 (2015).
 - [37] Y. Lee, E. Bersin, A. Dahlberg, S. Wehner, and D. Englund, npj Quantum Information **8**, 1 (2022).
 - [38] M. Campisi and R. Fazio, Nature communications **7**, 1 (2016).
 - [39] V. Mukherjee, U. Divakaran, A. del Campo, et al., Physical Review Research **2**, 043247 (2020).
 - [40] N. Y. Halpern, C. D. White, S. Gopalakrishnan, and G. Refael, Physical Review B **99**, 024203 (2019).
 - [41] S. I. Rapoport, Biophysical Journal **10**, 246 (1970).
 - [42] P. Bonifazi, M. Goldin, M. A. Picardo, I. Jorquera, A. Cattani, G. Bianconi, A. Represa, Y. Ben-Ari, and R. Cossart, Science **326**, 1419 (2009).
 - [43] E. Schneidman, M. J. Berry, R. Segev, and W. Bialek, Nature **440**, 1007 (2006).
 - [44] G. Buzsáki and K. Mizuseki, Nature Reviews Neuroscience **15**, 264 (2014).
 - [45] E. Gal, M. London, A. Globerson, S. Ramaswamy, M. W. Reimann, E. Muller, H. Markram, and I. Segev, Nature neuroscience **20**, 1004 (2017).
 - [46] R. Tönjes, C. E. Fiore, and T. Pereira, Nature Communications **12**, 1 (2021).
 - [47] H. Vroylandt, M. Esposito, and G. Verley, [EPL \(Europhysics Letters\)](#) **120**, 30009 (2017).
 - [48] T. Herpich, J. Thingna, and M. Esposito, [Phys. Rev. X](#) **8**, 031056 (2018).
 - [49] T. Herpich and M. Esposito, [Phys. Rev. E](#) **99**, 022135 (2019).
 - [50] M. Suñé and A. Imparato, [Phys. Rev. Lett.](#) **123**, 070601 (2019).
 - [51] J. M. Yeomans, Statistical mechanics of phase transitions (Clarendon Press, 1992).
 - [52] F. Y. Wu, [Rev. Mod. Phys.](#) **54**, 235 (1982).
 - [53] M. Blume, V. J. Emery, and R. B. Griffiths, [Phys. Rev. A](#) **4**, 1071 (1971).
 - [54] W. Hoston and A. N. Berker, [Phys. Rev. Lett.](#) **67**, 1027 (1991).
 - [55] D. T. Gillespie, The journal of physical chemistry **81**, 2340 (1977).
 - [56] H. B. Callen, “Thermodynamics and an introduction to thermostatistics,” (1998).
 - [57] S. R. Salinas, in [Introduction to Statistical Physics](#) (Springer, 2001) pp. 1–17.
 - [58] S. Liepelt and R. Lipowsky, [Phys. Rev. Lett.](#) **98**, 258102 (2007).
 - [59] S. Liepelt and R. Lipowsky, [Phys. Rev. E](#) **79**, 011917 (2009).
 - [60] K. Proesmans, B. Cleuren, and C. Van den Broeck, [Phys. Rev. Lett.](#) **116**, 220601 (2016).
 - [61] K. Proesmans and C. Van den Broeck, [Physical review letters](#) **115**, 090601 (2015).
 - [62] K. Proesmans, Y. Dreher, M. c. v. Gavrilov, J. Bechhoefer, and C. Van den Broeck, [Phys. Rev. X](#) **6**, 041010 (2016).
 - [63] K. Proesmans and C. E. Fiore, Physical Review E **100**, 022141 (2019).
 - [64] O. Kedem and S. R. Caplan, [Trans. Faraday Soc.](#) **61**, 1897 (1965).
 - [65] C. E. Fiore and M. G. E. da Luz, [The Journal of Chemical Physics](#) **138**, 014105 (2013), <https://doi.org/10.1063/1.4772809>.
 - [66] M. S. S. Challa, D. P. Landau, and K. Binder, [Phys. Rev. B](#) **34**, 1841 (1986).
 - [67] S. H. Strogatz, Nonlinear dynamics and chaos: with applications to physics, b (CRC press, 2018).